

## Research Article

# Synthesis of Novel $\text{Yb}_x\text{Sb}_{2-x}\text{Te}_3$ Hexagonal Nanoplates: Investigation of Their Physical, Structural, and Photocatalytic Properties

Younes Hanifehpour and Sang Woo Joo

WCU Nano Research Center, School of Mechanical Engineering, Yeungnam University, Gyeongsan 712-749, Republic of Korea

Correspondence should be addressed to Younes Hanifehpour; [younes.hanifehpour@gmail.com](mailto:younes.hanifehpour@gmail.com) and Sang Woo Joo; [swjoo@yu.ac.kr](mailto:swjoo@yu.ac.kr)

Received 22 November 2013; Revised 28 April 2014; Accepted 29 April 2014; Published 29 May 2014

Academic Editor: Gong-Ru Lin

Copyright © 2014 Y. Hanifehpour and S. W. Joo. This is an open access article distributed under the Creative Commons Attribution License, which permits unrestricted use, distribution, and reproduction in any medium, provided the original work is properly cited.

Yb-doped  $\text{Sb}_2\text{Te}_3$  nanomaterials were synthesized by a coreduction method in hydrothermal condition. Powder X-ray diffraction patterns indicate that the  $\text{Yb}_x\text{Sb}_{2-x}\text{Te}_3$  crystals ( $x = 0.00-0.05$ ) are isostructural with  $\text{Sb}_2\text{Te}_3$ . The cell parameter  $a$  decreases for  $\text{Yb}_x\text{Sb}_{2-x}\text{Te}_3$  compounds upon increasing the dopant content ( $x$ ), while  $c$  increases. Scanning electron microscopy and transmission electron microscopy images show that doping of  $\text{Yb}^{3+}$  ions in the lattice of  $\text{Sb}_2\text{Te}_3$  produces different morphology. The electrical conductivity of Yb-doped  $\text{Sb}_2\text{Te}_3$  is higher than the pure  $\text{Sb}_2\text{Te}_3$  and increases with temperature. By increasing concentration of the  $\text{Yb}^{3+}$  ions, the absorption spectrum of  $\text{Sb}_2\text{Te}_3$  shows red shifts and some intensity changes. In addition to the characteristic red emission peaks of  $\text{Sb}_2\text{Te}_3$ , emission spectra of doped materials show other emission bands originating from  $f-f$  transitions of the  $\text{Yb}^{3+}$  ions. The photocatalytic performance of as-synthesized nanoparticles was investigated towards the decolorization of Malachite Green solution under visible light irradiation.

## 1. Introduction

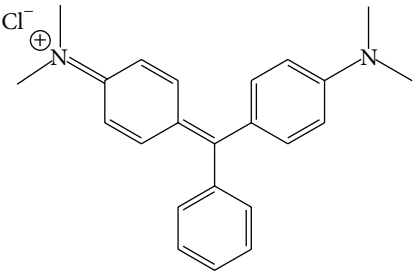
Antimony telluride ( $\text{Sb}_2\text{Te}_3$ ) based compounds are very promising materials for thermoelectric (TE) applications in solid-state refrigeration and power generation, [1–3] but their extensive application is hindered by their low thermoelectric efficiency. Antimony telluride is a semiconductor with narrow band gap and layered structure. Possessing intrinsically a high figure-of-merit (ZT) because of its large Seebeck coefficient, this compound and its doped derivatives are considered to be the best candidates for near room-temperature TE applications [4–7]. Rare earth ions doped nanomaterials have become an increasingly important research topic and opened up the opportunity for creating new applications in diverse areas, such as light emitting displays, biological labeling, and imaging [8–10]. Investigations of impurity effects or doping agents on the physical properties of  $\text{Sb}_2\text{Te}_3$  are attractive both for applied and basic research. Incorporating trivalent cations such as  $\text{Sb}^{3+}$  [11],  $\text{In}^{3+}$  [12],  $\text{Fe}^{3+}$  [13],  $\text{Mn}^{3+}$  [14], and some trivalent 3d elements [15] to the lattice of  $\text{Bi}_2\text{Se}_3$  has been reported. Also,  $\text{Ln}_x\text{Bi}_{2-x}\text{Se}_3$  ( $\text{Ln}$ :  $\text{Sm}^{3+}$ ,  $\text{Eu}^{3+}$ ,  $\text{Gd}^{3+}$ ,  $\text{Tb}^{3+}$ , and

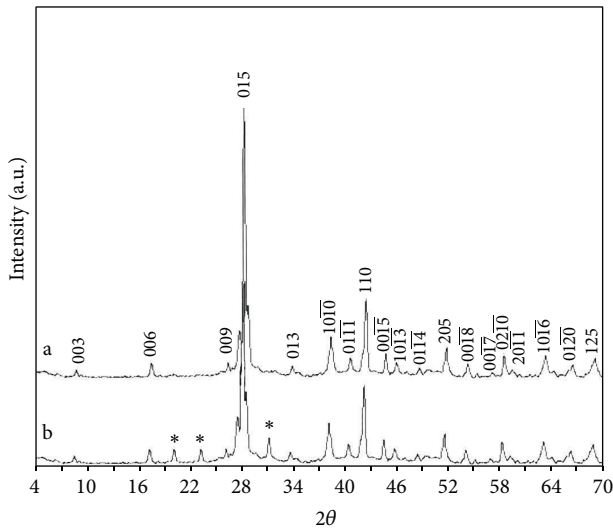
$\text{Nd}^{3+}$ ) based nanomaterials were prepared by Alemi et al. [16, 17]. Recently, we have synthesized new luminescent nanomaterials based on doping of lanthanide ( $\text{Ln}$ :  $\text{Ho}^{3+}$ ,  $\text{Nd}^{3+}$ , and  $\text{Lu}^{3+}$ ) into the lattice of  $\text{Sb}_2\text{S}_3$  and ( $\text{Ln}$ :  $\text{Ho}^{3+}$ ,  $\text{Nd}^{3+}$ ,  $\text{Lu}^{3+}$ ,  $\text{Sm}^{3+}$ ,  $\text{Er}^{3+}$ , and  $\text{Yb}^{3+}$ ) into the lattice of  $\text{Sb}_2\text{Se}_3$  [18–21]. To the best of our knowledge, there is no study about doping of rare earth cations into the lattice of  $\text{Sb}_2\text{Te}_3$ . The electronic properties of antimony telluride could be affected by doping of lanthanide ions into a Sb–Te framework. Herein, we report synthesis of  $\text{Yb}_x\text{Sb}_{2-x}\text{Te}_3$  nanomaterials by a hydrothermal route. Structural and spectroscopic properties and electrical and thermal conductivity of the as-prepared materials are described. Also, the photocatalytic activity of  $\text{Yb}_x\text{Sb}_{2-x}\text{Te}_3$  nanomaterials was investigated towards Malachite Green (as a model organic dye) decolorization under visible light irradiation.

## 2. Experimental

All chemicals were of analytical grade and were used without further purification. Tellurium powder, Sodium Borohydride,

TABLE I: Characteristics of Malachite Green.

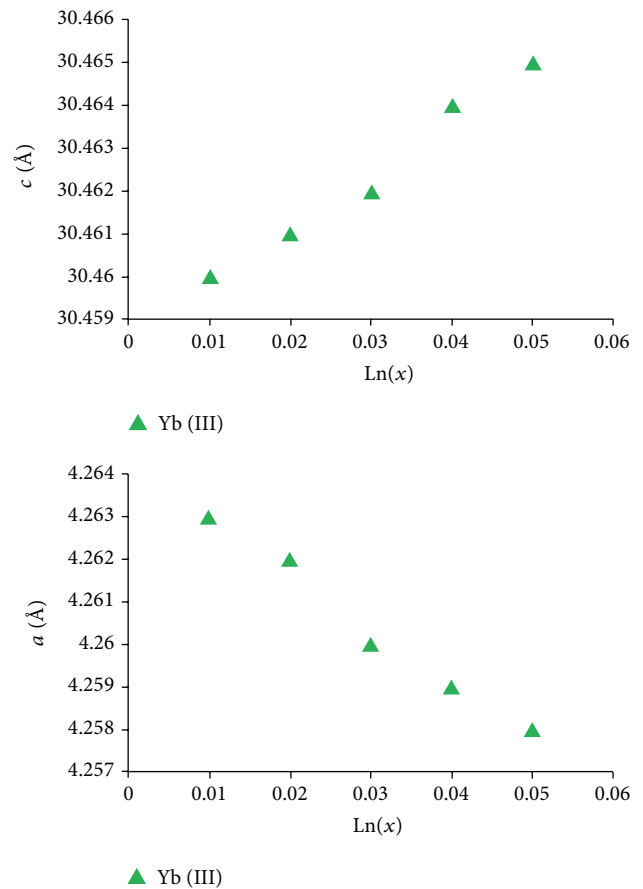
Color index name	Chemical structure	Molecular formula	Color index number	$\lambda_{\max}$ (nm)	$M_w$ (g/mol)
C.I. Basic Green-4		$C_{23}H_{25}N_2HCl$	42000	355	365

FIGURE 1: Powder X-ray diffraction pattern of (a)  $Yb_{0.05}Sb_{1.95}Te_3$  and (b) impure  $Sb_2Te_3$  synthesized at  $180^\circ C$  and 48 h.

$SbCl_3$ ,  $Yb_2O_3$ , NaOH, and Malachite Green were obtained from Merck. The characteristic of this dye is presented in Table I. Ethanol (99%).  $4H_2O$  were obtained from Aldrich.

### 3. Synthesis of $Sb_2Te_3$ and Yb-Doped $Sb_2Te_3$ Samples

Tellurium powder (0.382 g) and NaOH (0.6 g) were added to distilled water (60 mL) and stirred well for 10 min at room temperature. Afterwards, Sodium Borohydride (4 g),  $SbCl_3$ , and  $Yb_2O_3$  with appropriate ratios were added, and the mixture was transferred to a 100 mL Teflon-lined autoclave. The autoclave was sealed, maintained at  $180^\circ C$  for 48 h, and then allowed to cool to room temperature naturally. The as-synthesized  $Yb_xSb_{2-x}Te_3$  nanomaterials were collected and washed with distilled water and absolute ethanol several times in order to remove residual impurities and then dried at room temperature. The final black powders were obtained as a result.

FIGURE 2: The  $a$  and  $c$  lattice constants of  $Yb_xSb_{2-x}Te_3$  ( $0 \leq x \leq 0.05$ ) dependent upon  $Yb^{3+}$  doping on  $Sb^{3+}$  sites.

### 4. Characterization Methods

The products yields were 85–95%. X-ray powder diffractometer (XRD D5000 Siemens AG, Munich, Germany) with  $CuK_\alpha$  radiation was used for phase identification. The morphology of the materials was examined using a JEOL JSM-6700F Scanning Electron Microscope (SEM). A linked ISIS-300, Oxford EDS (energy dispersion spectroscopy) detector was used for elemental analyses. The SAED pattern and HRTEM image were performed by a Cs-corrected high-resolution TEM (JEM-2200FS, JEOL) operated at 200 kV.

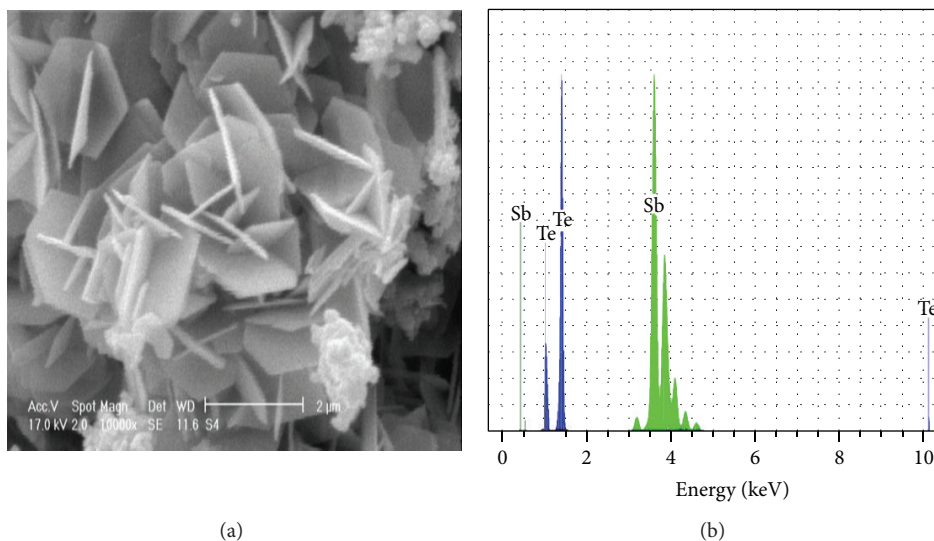


FIGURE 3: The SEM image (a) and EDX (b) of as-prepared  $\text{Sb}_2\text{Te}_3$  synthesized at  $180^\circ\text{C}$  and 48 h.

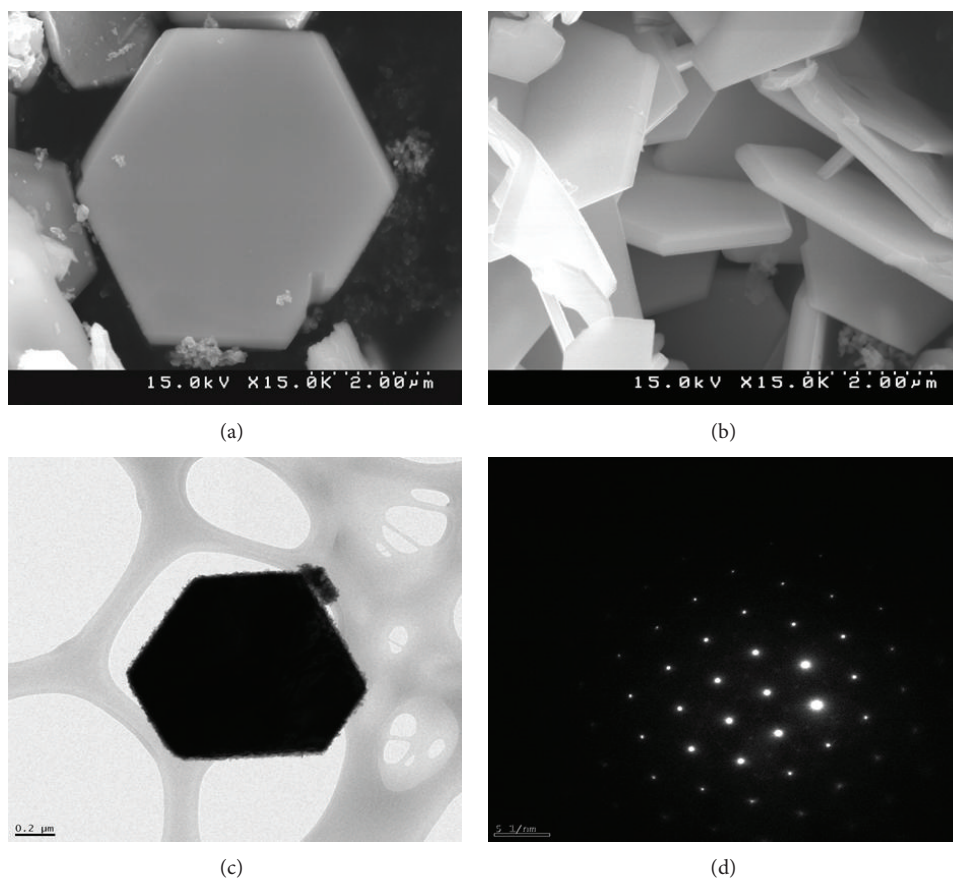


FIGURE 4: The SEM image (a and b), TEM image (c), and SAED pattern (d) of as-prepared  $\text{Yb}_{0.02}\text{Sb}_{1.98}\text{Te}_3$  nanoplates at different magnifications synthesized at  $180^\circ\text{C}$  and 48 h.

Photoluminescence measurements were carried out using a Spex FluoroMax-3 spectrometer. The absorption spectra were recorded with UV-Vis spectrophotometer (Varian Cary 3 Bio). The UV-Vis diffuse reflectance spectra were used for evaluation of photophysical properties of as-synthesized

material. The electrical and thermoelectrical resistivity of samples was measured by Four Probe Method. An oven was required for the variation of temperature of the samples from the room temperature to about  $200^\circ\text{C}$ . Small chip with 1 mm thickness and 7 mm length was used for this analysis. This

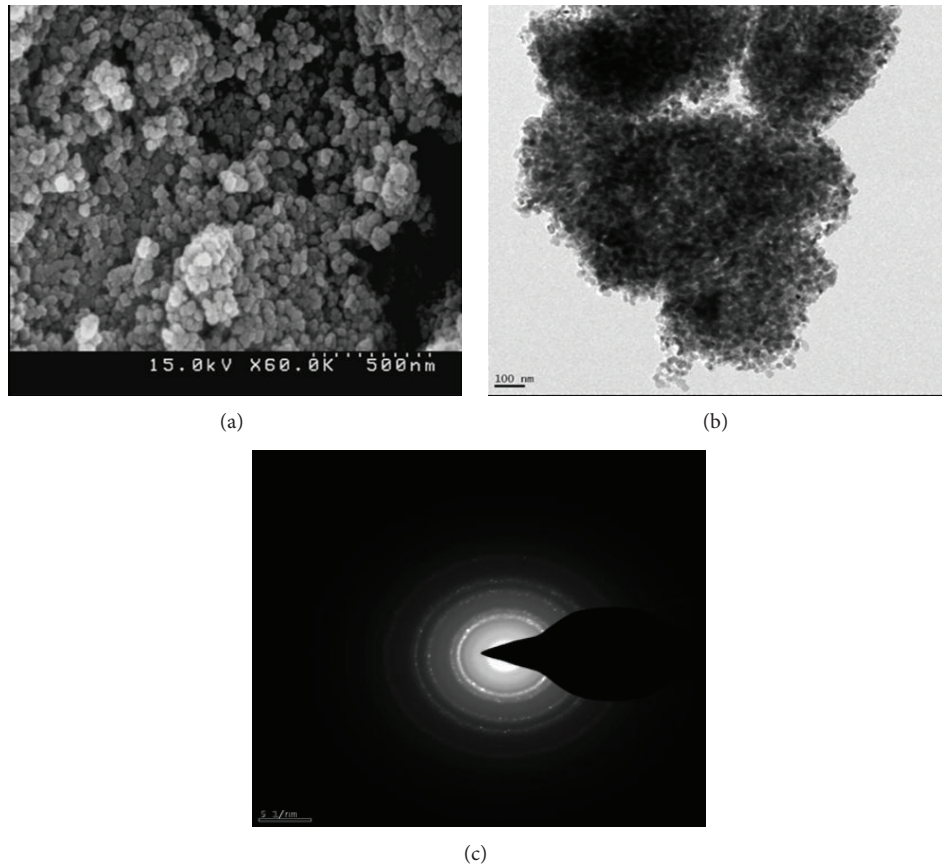


FIGURE 5: The SEM images (a), TEM image (b), and SAED pattern (c) of as-prepared  $\text{Yb}_{0.05}\text{Sb}_{1.95}\text{Te}_3$  nanoparticles at different magnifications.

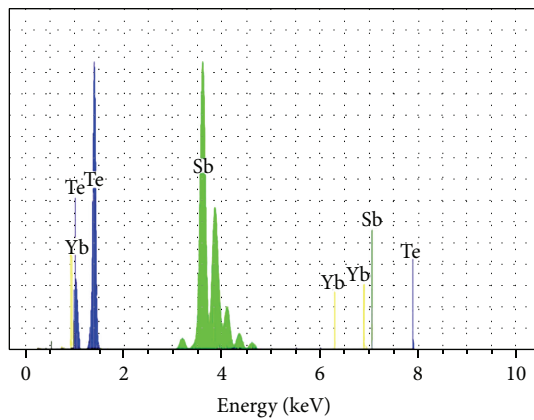


FIGURE 6: The EDX patterns of  $\text{Yb}_x\text{Sb}_{2-x}\text{Te}_3$  synthesized at  $180^\circ\text{C}$  and 48 h.

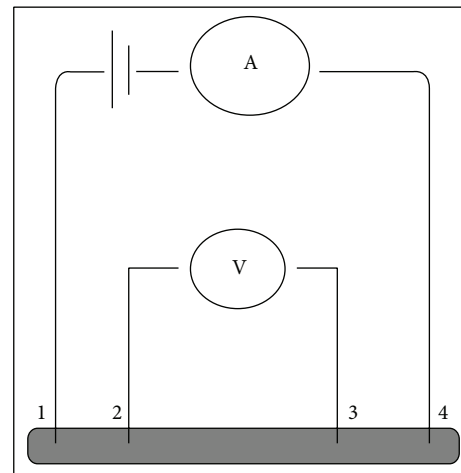


FIGURE 7: Schematic of four-point probe.

chip was obtained by pressing of 30 mg of sample under 30 kpa pressing device. Celref program (CCP14, London, UK) and WinXPOW program (STOE & CIE GmbH, Darmstadt, Germany) using a profile fitting procedure were used for calculation of cell parameters from powder XRD patterns and determination of reflections, respectively.

## 5. Photocatalytic Studies

The photocatalytic activity of undoped and  $\text{Yb}_x\text{Sb}_{2-x}\text{Te}_3$  nanomaterials was evaluated by the decolorization of Malachite Green (a triphenylmethane dye) in an aqueous solution under visible light. In a typical process, 0.1 g of the photocatalyst powder was added to 100 mL Malachite Green solution

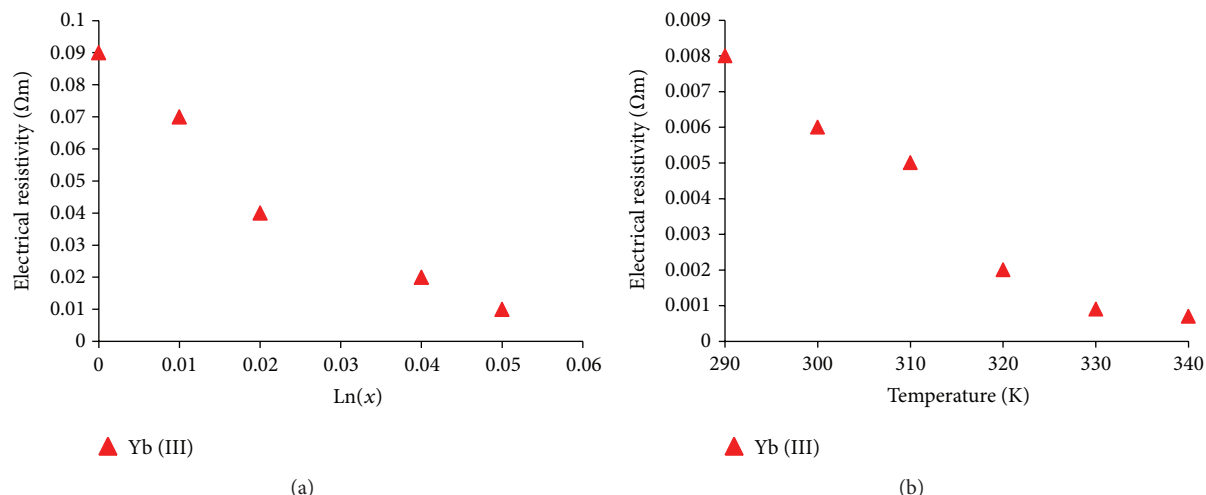


FIGURE 8: Electrical resistivity (a) and thermoelectrical resistivity (b) of  $\text{Yb}_x\text{Sb}_{2-x}\text{Te}_3$  nanomaterials at room temperature.

with an initial concentration of 5 mg/L. The suspension of photocatalyst and Malachite Green was magnetically stirred in a quartz photoreactor in the dark for 15 mins to establish an adsorption/desorption equilibrium of the dye. Then, the solution was irradiated by a 6 W fluorescent visible lamp (GK-140, China) as the light source. The color removal efficiency (CR (%)) was expressed as the percentage ratio of decolorized dye concentration to that of the initial one. During the photocatalytic process, 5 mL of the suspension was sampled at desired times and after centrifugation, the removal of color was evaluated by determining the absorbance of the solution at  $\lambda_{\text{max}} = 619 \text{ nm}$  by using UV-Vis spectrophotometer, Lightwave S2000 (England).

## 6. Results and Discussion

The lattice parameters were determined via reflections observed in  $2\theta = 4\text{--}70^\circ$ . An X-ray diffraction (XRD) pattern of the newly obtained Yb-doped  $\text{Sb}_2\text{Te}_3$  is shown in Figure 1(a). All peaks can be perfectly indexed to rhombohedral  $\text{Sb}_2\text{Te}_3$  (space group: R-3 m) with lattice constants  $a = 4.264 \text{ \AA}$  and  $c = 30.458 \text{ \AA}$  (Joint Committee on Powder Diffraction Standards (JCPDS) card number 15-0874). Additional unknown phases as shown by stars in Figure 1(b) were observed beyond doping levels of  $x = 0.05$  for  $\text{Yb}^{3+}$ .

The calculation of cell parameters of the as-prepared materials was done from the XRD patterns. By increasing dopant content ( $x$ ), the  $a$  parameter for  $\text{Yb}^{3+}$  decreases, while the  $c$  parameter increases, as shown in Figure 2. These changes of lattice constants can be attributed to the effective ionic radii of the  $\text{Yb}^{3+}$  ions and lattice shifts to various position of dopants or defects site. Figure 3 shows SEM image and EDX of  $\text{Sb}_2\text{Te}_3$  nanoplates. The thickness of these plates is around 40–80 nm. The EDX analysis of the product confirms the ratio of Sb/Te to be 2:3, as expected. Doping of various  $\text{Yb}^{3+}$  concentrations into the structure of  $\text{Sb}_2\text{Te}_3$  results in different morphology. At lower  $\text{Yb}^{3+}$  composition

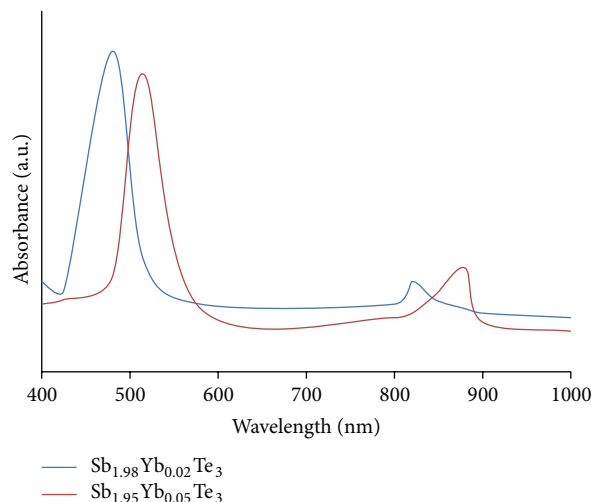


FIGURE 9: Absorption spectra of  $\text{Yb}_x\text{Sb}_{2-x}\text{Te}_3$  nanoparticles at room temperature.

the morphology is hexagonal nanoplate as seen in Figure 4 in which the thickness of plates is around 40–90 nm and at higher  $\text{Yb}^{3+}$  concentration the product is nanoparticles. Figure 4 shows SEM, TEM image, and SAED pattern of  $\text{Yb}_{0.05}\text{Sb}_{1.95}\text{Te}_3$  nanoparticles whose diameter is around 20–50 nm. The TEM image and SAED pattern of  $\text{Yb}_{0.02}\text{Sb}_{1.98}\text{Te}_3$  confirm the result of SEM and shows crystallinity of product as seen at Figure 5. As expected, the EDX analysis of the product confirms purity and the ratio of Sb/Te/Yb (see Figure 6). The electronic properties of antimony telluride could be affected by doping of lanthanide ions into a Sb–Te framework. Doping of lanthanide cations into  $\text{Sb}_2\text{Te}_3$  lattice results in decreasing the Sb–Te covalence bond. Due to different interaction in the doped  $\text{Sb}_2\text{Te}_3$  lattice, there are different growth directions in lattice and production of various morphologies. The Four Probe Method was used for the measurement of electrical and thermoelectrical resistivity

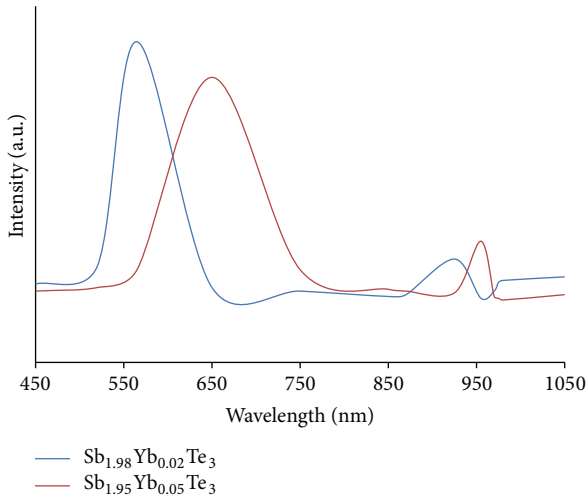


FIGURE 10: Photoluminescence spectra of  $\text{Yb}_x\text{Sb}_{2-x}\text{Te}_3$  nanoparticles at room temperature.

of samples (Figure 7). Figure 8(a) shows electrical resistivity of Yb-doped  $\text{Sb}_2\text{Te}_3$  nanomaterials. The electrical resistivity measured at room temperature for pure  $\text{Sb}_2\text{Te}_3$  was of the order of  $0.09 \Omega\cdot\text{m}$ . The minimum value of electrical resistivity for  $\text{Yb}^{3+}$ -doped compounds is  $0.008 \Omega\cdot\text{m}$ . Figure 8(b) shows the temperature dependence of the electrical resistivity for Yb-doped  $\text{Sb}_2\text{Te}_3$  between 290 and 340 K in which the electrical resistivity decreases with temperature. The minimum value of electrical resistivity for  $\text{Yb}_{0.05}\text{Sb}_{1.95}\text{Te}_3$  is  $0.0007 \Omega\cdot\text{m}$ . As a result, the electrical conductivity of Yb-doped  $\text{Sb}_2\text{Te}_3$  materials is higher than undoped  $\text{Sb}_2\text{Te}_3$  at room temperature and increases with temperature. Selected absorption spectra of  $\text{Sb}_{2-x}\text{Yb}_x\text{Te}_3$  ( $x = 0.02$  and  $0.05$ ) are shown in Figure 9. The DRS spectra of  $\text{Sb}_2\text{Te}_3$  lattice show an intensive peak around 480 nm. The absorption spectra in the spectral region 800–900 nm can be assigned to electronic transitions of  $\text{Yb}^{3+}$  from the  $^2F_{7/2}$  ground state to  $^2F_{5/2}$  excited level [22, 23]. As shown in Figure 9, there is a red shift in DRS spectra of  $\text{Sb}_{2-x}\text{Yb}_x\text{Te}_3$  compounds, respectively. The calculated band gaps from absorbance spectra for  $\text{Sb}_{2-x}\text{Yb}_x\text{Te}_3$  are  $E_g = 2.587 \text{ eV}$  (Yb-0.02) and  $2.48 \text{ eV}$  (Yb-0.05). Figure 10 exhibits the RT PL emission spectra of  $\text{Sb}_{2-x}\text{Yb}_x\text{Te}_3$  compounds. Two peaks are shown in the PL spectra of  $\text{Yb}^{3+}$ -doped compounds attributed to  $\text{Sb}_2\text{Te}_3$  lattice centered at 560 nm and another is assigned to  $f$ - $f$  transitions of  $\text{Yb}^{3+}$  ions from  $^2F_{5/2} \rightarrow ^2F_{7/2}$ . There are red shifts in PL spectra by increasing concentration of  $\text{Yb}^{3+}$  [22, 23]. Figure 11 shows the typical evolution of the absorption spectra of C.I. Basic Green-4 under the irradiation of visible light using the  $\text{Yb}_{0.05}\text{Sb}_{1.95}\text{Te}_3$  nanoparticles as a photocatalyst. The absorption peak around 355 nm gradually weakened and decreased from the absorption spectra, indicating the degradation of the BG4. The loss of absorbance may be due to the destruction of the azo band and dye chromogen. Since no new peak was observed, the BG4 has been decomposed. Also, the photocatalytic activity of synthesized undoped and Yb-doped  $\text{Sb}_2\text{Te}_3$  nanoparticles was compared and is presented in Figure 12. In a typical process, 100 mL

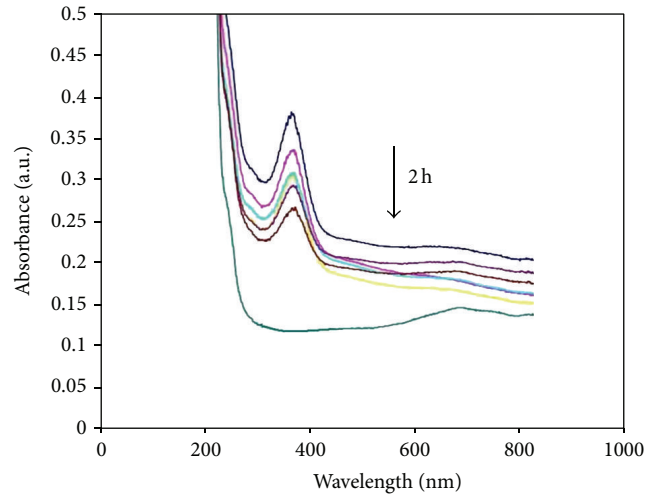


FIGURE 11: Absorption spectra of BG4 under the irradiation of visible light using the  $\text{Yb}_{0.05}\text{Sb}_{0.95}\text{Te}_3$  nanoparticles as a photocatalyst.

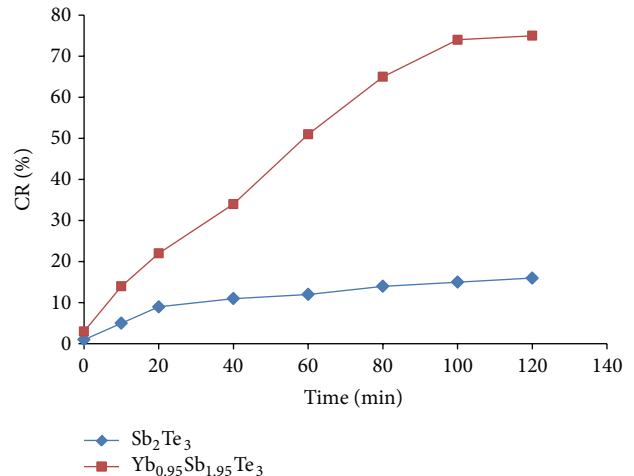


FIGURE 12: Color removal efficiency (CR (%)) for a 5 mg/L BG4 solution by photocatalytic process under visible light (catalyst loading 1.0 g/L).

of BG4 (5 mg/L) aqueous solution and 0.1 g of photocatalyst powder were mixed in a quartz photoreactor. It is clearly seen from Figure 12 that the color removal efficiency of the Yb-doped  $\text{Sb}_2\text{Te}_3$  catalyst is much higher than that of pure  $\text{Sb}_2\text{Te}_3$ . The results demonstrated the good photocatalytic ability of these nanoparticles under visible light and can be compared with other new catalysts [24–26]. As can be seen, the decolorization efficiency is 16.30 and 75.62% after 120 min of treatment for  $\text{Sb}_2\text{Te}_3$  and  $\text{Yb}_{0.05}\text{Sb}_{1.95}\text{Te}_3$ , respectively.

## 7. Conclusion

Novel thermoelectric  $\text{Yb}_x\text{Sb}_{2-x}\text{Te}_3$  based nanomaterials were synthesized by a simple and efficient coreduction method at 48 h and  $180^\circ\text{C}$  at basic media. According to SEM and TEM images, different morphologies were seen in Yb-doped

Sb<sub>2</sub>Te<sub>3</sub>. Lanthanide doping promotes the electrical conductivity of Sb<sub>2</sub>Te<sub>3</sub> as well as thermal conductivity. UV-Vis absorption and emission spectroscopy reveals mainly electronic transitions of the Yb<sup>3+</sup> doped nanomaterials. Red shifts as well as increasing of intensity of absorption and emission peaks were seen in doped nanomaterial. Experiments showed that the as-obtained nanoparticles have high photocatalytic activity under visible light irradiation. The decolorization efficiency of BG4 solution using these photocatalysts was 16.30 and 75.62% after 120 min of treatment for Sb<sub>2</sub>Te<sub>3</sub> and Yb<sub>0.05</sub>Sb<sub>1.95</sub>Te<sub>3</sub>, respectively.

## Conflict of Interests

The authors declare that there is no conflict of interests regarding the publication of this paper.

## Acknowledgment

This work is supported by the Grant 2011-0014246 of the National Research Foundation of Korea.

## References

- [1] W. Shi, L. Zhou, S. Song, J. Yang, and H. Zhang, "Hydrothermal synthesis and thermoelectric transport properties of impurity-free antimony telluride hexagonal nanoplates," *Advanced Materials*, vol. 20, no. 10, pp. 1892–1897, 2008.
- [2] W. Shi, J. Yu, H. Wang, and H. Zhang, "Hydrothermal synthesis of single-crystalline antimony telluride nanobelts," *Journal of the American Chemical Society*, vol. 128, no. 51, pp. 16490–16491, 2006.
- [3] W. Wang, D. Long, Y. Liang, G. Zhang, B. Zeng, and Q. He, "Conversion of hexagonal Sb<sub>2</sub>Te<sub>3</sub> nanoplates into nanorings driven by growth temperature," *Langmuir*, vol. 27, no. 2, pp. 815–819, 2011.
- [4] W. Wang, B. Poudel, J. Yang, D. Z. Wang, and Z. F. Ren, "High-yield synthesis of single-crystalline antimony telluride hexagonal nanoplates using a solvothermal approach," *Journal of the American Chemical Society*, vol. 127, no. 40, pp. 13792–13793, 2005.
- [5] B. Zhou, Y. Ji, Y.-F. Yang, X.-H. Li, and J.-J. Zhu, "Rapid microwave-assisted synthesis of single-crystalline Sb<sub>2</sub>Te<sub>3</sub> hexagonal nanoplates," *Crystal Growth and Design*, vol. 8, no. 12, pp. 4394–4397, 2008.
- [6] S. S. Garje, D. J. Eisler, J. S. Ritch, M. Afzaal, P. O'Brien, and T. Chivers, "A new route to antimony telluride nanoplates from a single-source precursor," *Journal of the American Chemical Society*, vol. 128, no. 10, pp. 3120–3121, 2006.
- [7] T.-S. Kim and B.-S. Chun, "Microstructure and thermoelectric properties of n- and p-type Bi<sub>2</sub>Te<sub>3</sub> alloys by rapid solidification processes," *Journal of Alloys and Compounds*, vol. 437, no. 1–2, pp. 225–230, 2007.
- [8] Y. Sun, Y. Chen, L. Tian et al., "Morphology-dependent upconversion luminescence of ZnO:Er<sup>3+</sup> nanocrystals," *Journal of Luminescence*, vol. 128, no. 1, pp. 15–21, 2008.
- [9] F. Wang, Y. Han, C. S. Lim et al., "Simultaneous phase and size control of upconversion nanocrystals through lanthanide doping," *Nature*, vol. 463, no. 7284, pp. 1061–1065, 2010.
- [10] T. Tachikawa, T. Ishigaki, J.-G. Li, M. Fujitsuka, and T. Majima, "Defect-mediated photoluminescence dynamics of Eu<sup>3+</sup>-doped TiO<sub>2</sub> nanocrystals revealed at the single-particle or single-aggregate level," *Angewandte Chemie, International Edition*, vol. 47, no. 29, pp. 5348–5352, 2008.
- [11] N. S. Patil, A. M. Sargar, S. R. Mane, and P. N. Bhosale, "Growth mechanism and characterisation of chemically grown Sb doped Bi<sub>2</sub>Se<sub>3</sub> thin films," *Applied Surface Science*, vol. 254, no. 16, pp. 5261–5265, 2008.
- [12] S. Augustine and E. Mathai, "Growth, morphology, and microindentation analysis of Bi<sub>2</sub>Se<sub>3</sub>, Bi<sub>1.8</sub>In<sub>0.2</sub>Se<sub>3</sub>, and Bi<sub>2</sub>Se<sub>2.8</sub>Te<sub>0.2</sub> single crystals," *Materials Research Bulletin*, vol. 36, no. 13–14, pp. 2251–2261, 2001.
- [13] P. Lošťák, Č. Drašar, I. Klichová, J. Navrátil, and T. Černohorský, "Properties of Bi<sub>2</sub>Se<sub>3</sub> single crystals doped with Fe atoms," *Physica Status Solidi B*, vol. 200, no. 1, pp. 289–296, 1997.
- [14] P. Janíček, C. Drasar, P. Losták, and J. Vejpravová, "Transport, magnetic, optical and thermodynamic properties of Bi<sub>2-x</sub>Mn<sub>x</sub>Se<sub>3</sub> single crystals," *Physica B*, vol. 403, no. 19–20, pp. 3553–3558, 2008.
- [15] P. Larson and W. R. L. Lambrecht, "Electronic structure and magnetism in Bi<sub>2</sub>Te<sub>3</sub>, Bi<sub>2</sub>Se<sub>3</sub>, and Sb<sub>2</sub>Te<sub>3</sub> doped with transition metals (Ti-Zn)," *Physical Review B*, vol. 78, no. 19, Article ID 195207, pp. 195207–195214, 2008.
- [16] A. Alemi, A. Babalou, M. Dolatyari, A. Klein, and G. Meyer, "Hydrothermal synthesis of Nd<sup>III</sup> doped Bi<sub>2</sub>Se<sub>3</sub> nanoflowers and their physical properties," *Zeitschrift für Anorganische und Allgemeine Chemie*, vol. 635, no. 12, pp. 2053–2057, 2009.
- [17] A. Alemi, A. Klein, G. Meyer, M. Dolatyari, and A. Babalou, "Synthesis of new Ln<sub>x</sub>Bi<sub>2-x</sub>Se<sub>3</sub> (Ln: Sm<sup>3+</sup>, Eu<sup>3+</sup>, Gd<sup>3+</sup>, Tb<sup>3+</sup>) nanomaterials and investigation of their optical properties," *Zeitschrift für Anorganische und Allgemeine Chemie*, vol. 637, no. 1, pp. 87–93, 2011.
- [18] A. Alemi, Y. Hanifehpour, S. W. Joo, A. Khandar, A. Morsali, and B.-K. Min, "Co-reduction synthesis of new Ln<sub>x</sub>Sb<sub>2-x</sub>S<sub>3</sub> (Ln: Nd<sup>3+</sup>, Lu<sup>3+</sup>, Ho<sup>3+</sup>) nanomaterials and investigation of their physical properties," *Physica B: Condensed Matter*, vol. 406, no. 14, pp. 2801–2805, 2011.
- [19] A. Alemi, Y. Hanifehpour, S. W. Joo, and B.-K. Min, "Structural studies and physical properties of novel Sm<sup>3+</sup>-doped Sb<sub>2</sub>Se<sub>3</sub> nanorods," *Physica B: Condensed Matter*, vol. 406, no. 20, pp. 3831–3835, 2011.
- [20] A. Alemi, Y. Hanifehpour, S. W. Joo, A. Khandar, A. Morsali, and B.-K. Min, "Synthesis and characterization of new Ln<sub>x</sub>Sb<sub>2-x</sub>S<sub>3</sub> (Ln: Yb<sup>3+</sup>, Er<sup>3+</sup>) nanoflowers and their physical properties," *Physica B: Condensed Matter*, vol. 407, no. 1, pp. 38–43, 2012.
- [21] A. Alemi, Y. Hanifehpour, S. W. Joo, and B.-K. Min, "Synthesis of novel Ln<sub>x</sub>Sb<sub>2-x</sub>S<sub>3</sub> (Ln: Lu<sup>3+</sup>, Ho<sup>3+</sup>, Nd<sup>3+</sup>) nanomaterials via co-reduction method and investigation of their physical properties," *Colloids and Surfaces A: Physicochemical and Engineering Aspects*, vol. 390, no. 1–3, pp. 142–148, 2011.
- [22] E. Loh, "4f<sup>n</sup> → 4f<sup>n-1</sup>5d absorption spectra of rare-earth ions," *Physical Review Letters*, vol. 175, pp. 533–536, 1968.
- [23] Y. Huang, W. Zhub, X. Feng, G. Zhaoc, and G. Huangc, "Spectroscopic properties of Yb<sup>3+</sup>-doped PbWO<sub>4</sub> single crystal," *Materials Letters*, vol. 58, pp. 159–162, 2003.
- [24] A. Khataee, A. Khataee, M. Fathinia, Y. Hanifehpour, and S. W. Joo, "Kinetic and mechanism of enhanced photocatalytic activity under visible light using synthesized Pr<sub>x</sub>Cd<sub>1-x</sub>Se nanoparticles," *Industrial & Engineering Chemistry Research*, vol. 52, no. 37, pp. 13357–13369, 2013.

- [25] A. Khataee, Y. Hanifehpour, M. Safarpour, and M. Hosseini, "Synthesis and characterization of  $\text{Er}_x\text{Zn}_{1-x}\text{Se}$  nanoparticles: a novel visible light responsive photocatalyst," *Science and Technology of Advanced Materials*, vol. 5, pp. 1–9, 2013.
- [26] A. Khataee, S. Fathinia, M. Fathinia, Y. Hanifehpour, S. W. Joo, and B. Soltani, "Synthesis, characterization and photocatalytic properties of nanostructured Sm-CdSe," *Current Nanoscience*, vol. 9, no. 6, pp. 780–786, 2013.





**Hindawi**

Submit your manuscripts at  
<http://www.hindawi.com>

